

PAPER

[View Article Online](#)
[View Journal](#) | [View Issue](#)Cite this: *Catal. Sci. Technol.*, 2021,
11, 624

Vanadium complexes derived from oxacalix[6]arenes: structural studies and use in the ring opening homo-/co-polymerization of ϵ -caprolactone/ δ -valerolactone and ethylene polymerization†

Tian Xing,^a Timothy J. Prior,^a Mark R. J. Elsegood,^b Nina V. Semikolenova,^c
Igor E. Soshnikov,^{cd} Konstantin Bryliakov,^{cd} Kai Chen^{ae} and Carl Redshaw^{id *a}

Reaction of $\text{Na}[\text{VO}(\text{tBuO})_4]$ (generated *in situ* from VOCl_3 and NaOtBu) with *p*-tert-butyltetrahydrodioxacalix[6]arene- H_6 (L^1H_6) afforded, after work-up (in MeCN), the mixed-metal complex $[(\text{VO})_2(\mu\text{-O})\text{Na}_2(\text{L}^1)(\text{MeCN})_4]\cdot 5(\text{MeCN})$ (**1**·5MeCN), whilst the oxo complex $[(\text{VO})_4\text{L}^1]$ (**2**·6MeCN) was isolated via the use of $[\text{VO}(\text{OnPr})_3]$. Reaction of L^1H_6 with $[\text{V}(\text{Np-CH}_3\text{C}_6\text{H}_4)(\text{OtBu})_3]$ afforded the complex $[(\text{V}(\text{Np-CH}_3\text{C}_6\text{H}_4)_2\text{L}^1)]$ (**3**·7MeCN·0.5CH₂Cl₂). Use of similar methodology afforded the imido complexes $[(\text{V}(\text{Np-RC}_6\text{H}_4)_2\text{L}^1)]$ (R = OMe (**4**); CF₃ (**5**); Cl (**6**); F (**7**)); on one occasion, reaction of $[\text{V}(\text{Np-CH}_3\text{C}_6\text{H}_4)(\text{OEt})_3]$ with L^1H_6 afforded the product $[(\text{VO}(\text{L}^2)_2\cdot 4\text{MeCN})]$ (**8**·4MeCN) ($\text{L}^2 = 2\text{-(p-CH}_3\text{-C}_6\text{H}_4\text{NCH)}\text{-4-tBu-C}_6\text{H}_2\text{O-6-CH}_2\text{)-4-tBuC}_6\text{H}_2\text{OH}$) in which L^1 has been cleaved. For comparative catalytic ring opening polymerization (ROP) studies, the known complexes $[(\text{VOL}^3)]$ ($\text{L}^3 = \text{oxacalix[3]arene}$) (**I**), $[(\text{V}(\text{Np-CH}_3\text{-C}_6\text{H}_4)_2\text{L}^3)]$ (**II**), $[(\text{Li}(\text{MeCN})_4)]$ $[(\text{V}_2(\text{O})_2\text{Li}(\text{MeCN})(\text{L}^6\text{H}_2)_2)]$ ($\text{L}^6\text{H}_6 = p\text{-tert-butylcalix[6]areneH}_6$) (**III**) and $[(\text{VO})_2\text{L}^8\text{H}]$ ($\text{L}^8\text{H}_8 = p\text{-tert-butylcalix[8]areneH}_8$) (**IV**) have also been prepared. ROP studies, with or without external alcohol present, indicated that complexes **1** to **8** exhibited moderate to good conversions for ϵ -CL, δ -VL and the co-polymerization thereof. Within the imido series, a positive influence was observed when electron withdrawing substituents were present. These systems afforded relatively low molecular weight products and were also inactive toward the ROP of *rac*-lactide. In the case of ethylene polymerization, complexes **3**, **5** and **7** exhibited highest activity when screened in the presence of dimethylaluminium chloride/ethyltrichloroacetate; the activity of **4** was much lower. The products were highly linear polyethylene with M_w in the range 74–120 $\times 10^3$ Da.

Received 10th October 2020,
Accepted 19th November 2020

DOI: 10.1039/d0cy01979h

rsc.li/catalysis

Introduction

The need for new environmentally friendly plastics has been highlighted by on-going global pollution issues,

however traditional plastics, when used and disposed of correctly, still have a large part to play in society. Indeed, the recent COVID19 outbreak is a good illustration of our dependence on plastics, where there was widespread demand for the use of plastic-based facemasks.¹ Metal catalysts play a central role in the production of both petroleum-based plastics (α -olefin polymerization) and biodegradable polymers formed *via* the ring opening polymerization (ROP) of cyclic esters.² For both processes, manipulation of the catalyst properties can be achieved by variation of the metal-bound groups, and this allows for control over both catalytic activity and polymer properties. It is also important that the catalytic metal centre employed is cheap and non-toxic. With this in mind, a number of earth-abundant metals have been employed as the reactive metal centre in both polymerization processes.^{1,3} Furthermore, results using vanadium-based systems indicate this metal also has potential in this

^a Plastics Collaboratory, Department of Chemistry, University of Hull, Cottingham Road, Hull, HU6 7RX, UK. E-mail: c.redshaw@hull.ac.uk^b Chemistry Department, Loughborough University, Loughborough, Leicestershire, LE11 3TU, UK^c Borkov Institute of Catalysis, Pr. Lavrentieva 5, Novosibirsk 630090, Russian Federation^d Novosibirsk State University, Pirogova 1, Novosibirsk 630090, Russian Federation^e Collaborative Innovation Center of Atmospheric Environment and Equipment Technology, Jiangsu Key Laboratory of Atmospheric Environment Monitoring and Pollution Control, School of Environmental Science and Engineering, Nanjing University of Information Science & Technology, Nanjing 210044, P. R. China† Electronic supplementary information (ESI) available. CCDC 1998549–1998555 (**1**·5MeCN, **2**·6MeCN, **3**·7MeCN·0.5CH₂Cl₂, **4**·4MeCN, **5**, **6**, **8**·4MeCN) contain the supplementary crystallographic data. For ESI and crystallographic data in CIF or other electronic format see DOI: 10.1039/d0cy01979h

area,⁴ and it is noteworthy that reports on the effect of imido ligand variation in vanadium-based systems have appeared for studies on oligo-/polymerization of ethylene, ethylene/propylene copolymerization and ethylene/cyclic olefin copolymerization.⁵ The ligands in the pre-catalyst can take a number of forms, selected in-part for their ability to impose some stability to the catalytically active species. In α -olefin polymerization, an external alkylating co-catalyst is typically employed to form a metal-alkyl [M-R] species, whilst in ROP, the generation of metal alkoxide [M-OR] species is favoured. Calix[*n*]arenes, which are phenolic macrocycles, have shown potential in a variety of catalytic applications.⁶ By variation of *n*, the number of phenolic groups, calix[*n*]arenes can act as platforms for binding multiple metal centres.⁷ In our previous work, a series of vanadium-based calix[*n*]arene complexes were structurally identified, and by changing the calixarene bridging group from a methylene ($-\text{CH}_2-$) to a dimethyleneoxa group ($-\text{CH}_2\text{OCH}_2-$), vanadium complexes with superior catalytic performance for both α -olefin homo- and co-polymerization over related methylene-bridged systems were obtained.⁸ These vanadium studies previously focused on oxacalix[3]arene derivatives, however larger oxacalix[*n*]arenes are known.⁹ Herein, we investigate the use of the *p*-*tert*-butyltetrahomodioxacalix[6]areneH₆-derived systems (Chart 1) in both the ROP of the cyclic esters ϵ -caprolactone and δ -valerolactone, and the copolymerization thereof, and for the polymerization of ethylene. Results are compared *versus* known vanadium catalysts bearing either *p*-*tert*-butylhexahomotrioxacalix[3]areneH₃ or *p*-*tert*-butylcalix[6] and 8]areneH_{6,8}-derived ligands (Chart 2).^{7,8,10} We note that poly(ϵ -caprolactone), PCL and PVL are favoured polymers given their biodegradability and the fact that they are considered as potential environmentally friendly commodity plastics.¹¹

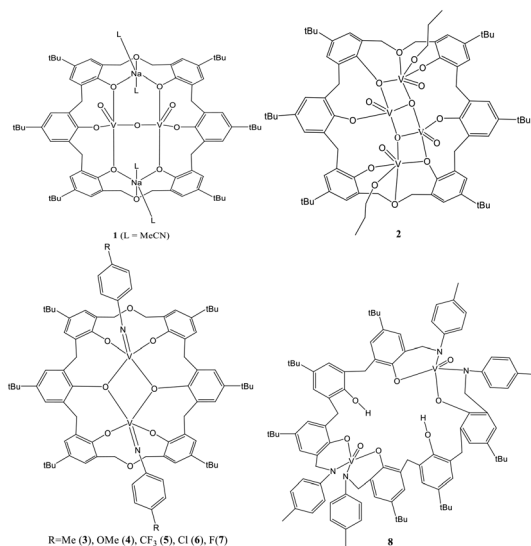


Chart 1 The pre-catalysts 1-8 prepared herein.

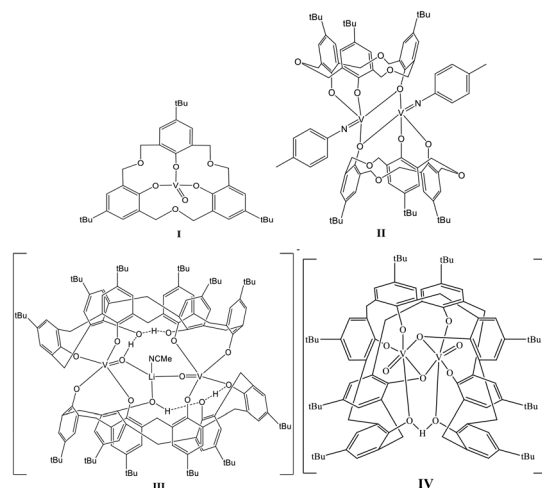


Chart 2 Known pre-catalysts I-IV used herein.^{7,9}

Results and discussion

Syntheses and solid-state structures

Oxo complexes. The heterobimetallic vanadium(V)/alkali metal reagent $[\text{NaVO}(\text{OtBu})_4]$, was synthesised by an adaptation of a procedure described by Wilkinson and co-workers,¹² whereby $[\text{VOCl}_3]$ and four equivalents of NaOtBu were stirred in diethylether (or THF) at -78°C for 12 h. *In situ* reaction of this vanadyl salt (two equivalents) with *p*-*tert*-butyltetrahomodioxacalix[6]areneH₆, L¹H₆ afforded, following work up (acetonitrile) and standing at 0°C , dark green blocks, which proved suitable for single crystal X-ray diffraction. The complex was found to be $[(\text{VO})_2(\mu\text{-O})\text{Na}_2(\text{L}^1)(\text{MeCN})_4]\cdot 5(\text{MeCN})$ (1.5MeCN), and the molecular structure of 1.5MeCN is shown in Fig. 1, with selected bond lengths and angles given in the caption. The complex contains two trigonal bipyramidal vanadyl centres, for which the $\text{V}=\text{O}$ bond length is typical at $1.588(3)\text{ \AA}$,¹⁰ linked *via* near linear ($171.8(2)^\circ$) $\text{V}-\text{O}11-\text{V}$ bonding. Each vanadium is further coordinated by three phenoxide oxygens of the oxacalix[6]arene, with longer bonding (*ca.* 1.95 \AA) observed to each of the bridging calixarene oxygens (O2 and O8) which are also involved in

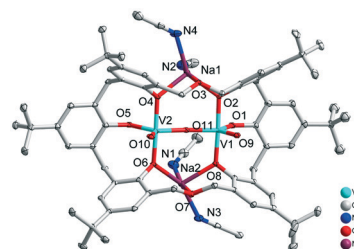


Fig. 1 Molecular structure of $[(\text{VO})_2(\mu\text{-O})\text{Na}_2(\text{L}^1)(\text{MeCN})_4]\cdot 5(\text{MeCN})$ (1.5MeCN) (H atoms and free MeCN molecules are omitted for clarity). Selected bond lengths (Å) and angles ($^\circ$): V1-O1 1.832(3), V1-O2 1.946(3), V1-O8 1.949(3), V1-O9 1.588(3), V1-O11 1.825(3), Na1-O2 2.231(3), Na1-O3 2.427(4), Na1-O4 2.232(4), Na1-N2 2.459(6), Na1-N4 2.396(5); O1-V1-O2 $87.74(14)$, O1-V1-O9 $112.40(16)$, O2-V1-O8 $176.37(14)$, V1-O11-V2 $171.8(2)$, O2-Na1-O4 $107.28(13)$.

bonding to a 5-coordinate sodium cation, with the latter (Na1 and Na2) each bonding to two of the phenoxide oxygens and the oxygen of the dimethyleneoxa bridge. Two acetonitrile ligands complete the bonding at each sodium centre.

Reaction of $[\text{VO}(\text{OnPr})_3]$ (4 equivalents) with L^1H_6 led, after work-up, to the blue complex $\{[\text{VO}_4\text{L}^1]_4\cdot 6\text{MeCN}$ ($2\cdot 6\text{MeCN}$). The molecular structure is shown in Fig. 2, with selected bond lengths and angles given in the caption. Calixarenes bind four vanadyl centres which form a 3-step V_4O_4 ladder. Such ladders have been observed previously in titanium calixarene chemistry.¹³

Two of the vanadyl centres (V1) are distorted octahedral and are bound by a long V–O2 bond (2.3732(14) Å) involving the oxygen of the dimethyleneoxa bridge *trans* to the vanadyl group, two phenoxides (1.7934(14) and 1.8128(14) Å) and an *n*-propoxide (V1–O8 1.7869(14) Å). The other vanadyl centre (V2) is trigonal bipyramidal ($\tau = 0.18$),¹⁴ and is linked to V1 *via* a triply bridging oxygen O6 (Fig. 2).

Imido complexes. Given that the oxo group is isoelectronic with the imido group,¹⁵ and that the latter can provide a useful NMR handle and can also be varied to alter the electronics, and to a lesser degree the sterics of the system,⁵ we also prepared a number of organoimido-containing vanadium complexes derived from L^1H_6 . Our entry into this chemistry is *via* the organoimido tris-alkoxides of the type $[\text{V}(\text{NAr})(\text{OR})_3]$ (R = *t*Bu, *i*Pr, *n*Pr or Et) which are readily available either *via* the use of $[\text{V}(\text{Np-RC}_6\text{H}_4)\text{Cl}_3]$ and subsequent addition of KOtBu ,¹⁶ or *via* the addition of ArNCO to $[\text{VO}(\text{OR})_3]$.¹⁷ Both routes have been utilized herein.

Interaction of $[\text{V}(\text{Np-CH}_3\text{C}_6\text{H}_4)(\text{OtBu})_3]$ with L^1H_6 led, following work-up, to the isolation of the complex $\{[\text{V}(\text{Np-CH}_3\text{C}_6\text{H}_4)]_2\text{L}^1\}$ ($3\cdot 7\text{MeCN}\cdot 0.5\text{CH}_2\text{Cl}_2$). Single crystals were grown from a saturated acetonitrile solution at ambient temperature and an X-ray structure determination revealed the structure shown in Fig. 3; selected bond lengths and angles are given Table 1. Each vanadium adopts a distorted

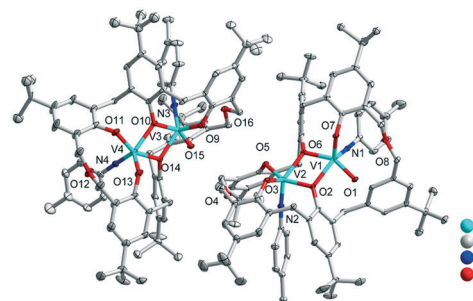


Fig. 3 Molecular structure of $\{[\text{V}(\text{Np-CH}_3\text{C}_6\text{H}_4)]_2\text{L}^1\}$ ($3\cdot 7\text{MeCN}\cdot 0.5\text{CH}_2\text{Cl}_2$). (H atoms and CH_2Cl_2 molecules are omitted for clarity).

squared-based pyramidal geometry with the near-linear imido ligand at the trigonal bipyramidal ($\tau = 0.11$),¹⁴ and are linked *via* asymmetric aryloxy bridges (of the dioxacalix[6]arene).

Replacement of the *para* methyl group by OMe (4), CF_3 (5), Cl (6) and F (7) led to the formation of the complexes 4–7 adopting the same general dimeric structure as observed for 3 (for synthetic details see the experimental section). The geometrical parameters (Table 1), show the similarity between these molecules and the *p*-tolyl analogue. The molecular structures of 4–6 are given in the ESI† (Fig. S1). As reported by Maatta *et al.*,¹⁶ the ^{51}V NMR shifts are very sensitive to the nature of the *para* substituent in such imido complexes (Fig. 4). In general, the trend observed herein is as observed by Maatta, with the electron donating groups (*e.g.* *p*-OMe) at low field *versus* electron withdrawing groups (*e.g.* *p*- CF_3) at high field. The exception is the *p*-F derivative, which surprisingly is found at low field (–173.4 ppm) and we tentatively attribute this to its position in relation to the macrocycle conformation.

When the metal precursor employed was $[\text{V}(\text{Np-CH}_3\text{C}_6\text{H}_4)(\text{OEt})_3]$, reaction with L^1H_6 led to the formation of small yellow prisms of $[\text{VO}(\text{L}^2)]_2\cdot 4\text{MeCN}$ ($8\cdot 4\text{MeCN}$) ($\text{L}^2 = 2\text{-}(p\text{-}$

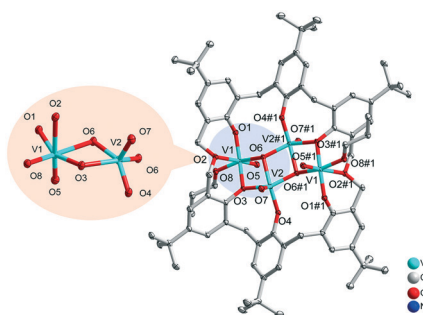


Fig. 2 View of the molecular structure of $\{[\text{VO}_4\text{L}^1]\}$ ($2\cdot 6\text{MeCN}$) (H atoms and free MeCN molecules are omitted for clarity; symmetry codes: #1: $1 - x, 1 - y, 1 - z$). Selected bond lengths V1–O1 1.8128(14), V1–O2 2.3732(14), V1–O3 2.0152(13), V1–O5 1.5866(15), V1–O6 2.0667(14), V1–O8 1.7869(14), V2–O3 1.9977(13), V2–O4 1.7934(14), V2–O6 1.9822(14), V2–O7 1.5830(15); O5–V1–O8 99.86(7), O5–V1–O1 100.97(7), O8–V1–O1 102.34(6), O5–V1–O3 101.19(7), O8–V1–O3 89.29(6), O1–V1–O3 152.74(6), O5–V1–O6 95.07(7), O8–V1–O6 157.22(6), O1–V1–O6 91.50(6), O3–V1–O6 70.89(5), O5–V1–O2 177.99(6), V2–O3–V1 107.25(6).

Table 1 Selected bond lengths (Å) and angles (°) for 3–6

Bond	3·7MeCN·0.5CH ₂ Cl ₂	4·4MeCN	5	6
V1–O1	1.837(3)	1.852(15)	1.786(4)	1.826(4)
V1–O2	2.095(3)	—	—	—
V1–O3	—	1.789(14)	1.815(4)	1.782(4)
V2–O4	—	2.068(15)	2.015(4)	2.010(4)
V2–O5	1.839(3)	1.841(16)	1.775(4)	1.836(4)
V2–O7	—	1.785(15)	1.818(4)	1.794(4)
V1–N1	1.652(3)	1.656(18)	1.645(5)	1.665(5)
V1–O6	2.016(3)	—	—	—
V1–O7	1.786(3)	—	—	—
V1–O1–C1	123.2(2)	123.00(12)	127.2(3)	122.7(4)
V1–O1–C58	129.3(2)	—	—	—
V1–O8–C58	—	128.44(12)	120.9(3)	127.4(3)
V1–O2–V2	108.34(11)	—	—	—
V1–O6–V2	110.10(11)	—	—	—
V2–O4–V1	—	108.68(7)	109.14(19)	108.7(2)
V1–O8–V2	—	109.05(7)	108.65(19)	108.5(2)
V1–N1–C70	173.7(3)	—	—	169.5(5)
V1–N1–C71	—	176.51(16)	175.9(5)	—
V2–N2–C81	—	178.53(17)	174.5(5)	—
V1–N2–C76A	—	—	—	174.0(4)



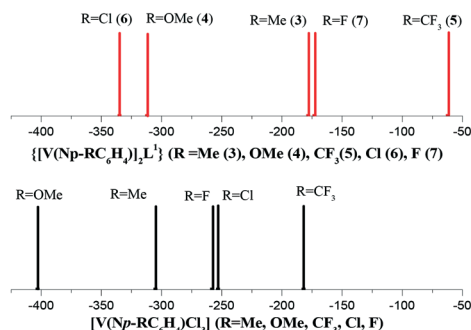


Fig. 4 ^{51}V NMR chemical shifts for **3–7** and $[\text{V}(\text{Np-RC}_6\text{H}_4)\text{Cl}_3]$ ($\text{R} = \text{Me}$, OMe , CF_3 , Cl , F).¹⁶

$\text{CH}_3\text{C}_6\text{H}_4\text{NCH})$ -4-*t*Bu- $\text{C}_6\text{H}_2\text{O}$ -6- CH_2)-4-*t*Bu $\text{C}_6\text{H}_2\text{OH}$). The molecular structure of **8**, as determined using synchrotron radiation, is shown in Fig. 5, with selected bond lengths and angles given in the caption. The molecule sits on a centre of symmetry. Interestingly, the dioxacalix[6]arene has been split in two by a reaction of the bridging oxygens and the *p*-tolylimido groups. The result is a metallo-macrocycle containing two square-based pyramidal vanadyl centres. The vanadyl $\text{V}=\text{O}$ bond length is typical at 1.5933(4) Å,¹⁰ whilst the phenoxide bond lengths at 1.8891(15) and 1.9046(15) Å are comparable with those observed elsewhere in vanadyl calixarene chemistry.^{7,10} The two uncoordinated phenolic OH groups are involved in H-bonding to vanadium-bound phenoxide groups. There are four solvent molecules (MeCN) of crystallization per molecule, with two residing inside the metallo-macrocycle. We note that calixarene cleavage is rare, with previous reports involving cleavage of a methylene bridge under acidic conditions.¹⁸

Ring opening polymerization studies

General: The performance of these complexes to act as catalysts for the ring opening polymerization (ROP) of ϵ -caprolactone (ϵ -CL) (Table S1, ESI[†]), δ -valerolactone (δ -VL) (Table S2, ESI[†]), both with and without one equivalent of benzyl alcohol (BnOH) per vanadium present, has been investigated.

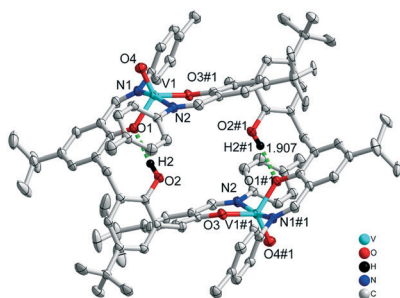


Fig. 5 View of the molecular structure of $[\text{VO}(\text{L}^2)]_2 \cdot 4\text{MeCN}$ (**8**·4MeCN) (H atoms and MeCN molecules are omitted for clarity) ($\text{L}^2 = 2$ -(*p*- CH_3 - $\text{C}_6\text{H}_4\text{NCH})$ -4-*t*Bu- $\text{C}_6\text{H}_2\text{O}$ -6- CH_2)-4-*t*Bu $\text{C}_6\text{H}_2\text{OH}$). Selected bond lengths (Å) and angles (°): V1–O1 1.9046(15), V1–O3A 1.8891(15), V1–O4 1.5933(17), V1–N1 2.1192(18), V1–N2A 2.1118(19), V1–O1–C9 131.18(14), V1–O3–C31 131.67(13), V1–N1–C1 117.87(19), V1–N1–C(8) 124.00(15).

Results in the absence of BnOH were less controlled but for completion are presented in the ESI[†] (Tables S1 and S2). The co-polymerization of ϵ -caprolactone and δ -valerolactone (Table 4) has also been investigated. In each case, performances are compared against the known complexes **I–IV** (Chart 2).

ϵ -Caprolactone (ϵ -CL)

Complexes **1–8** and **I–IV** were screened for their ability to polymerise ϵ -caprolactone and the results are collated in Table 2. The polymerization screening indicated that the best conditions were 500 equivalents of ϵ -caprolactone to vanadium at 130 °C. The activity of complex **1** increased with temperature and peaked at 500 equivalents of monomer. Complex **1** was also active at low catalyst loading leading to 82.5% conversion after 8 h for 1000 equivalents of monomer.

The observed activity of complex **1** surpassed that of the other complexes screened herein, and this was attributed to the additional presence of the sodium centres.

All polymers obtained were of low polydispersity ($\text{PDI} < 1.6$), which suggested that these polymerizations occurred without significant side reactions. Interestingly, only low molecular weight polymers were obtained using these oxovanadium/imido vanadium systems.

The screening of complexes **1–8** and **I–IV** (Table 2) revealed that the vanadium-based L^1 or L^2 -containing complexes namely **1**, **5**, **6** and **8** herein, exhibited higher activities than the known complexes **I–IV** under the conditions employed. After 24 h (Table 1), complexes **2**, **I**, **II**, **III**, **IV** afforded relatively lower conversions ($< 90\%$), whereas higher conversions ($> 90\%$) were reached using complexes **1**, **3–7**, **8**, under similar conditions. From a kinetic study (Fig. 6a), it was observed that the PCL polymerization rate followed the order: **1** $>$ **8** $>$ **II** $>$ **I** $>$ **III** \approx **3** $>$ **2** $>$ **IV**. For complexes within the imido-alkoxide family, the kinetic and TON/TOF results (Table 2, Fig. 6b) showed that the catalytic activity followed the order: **5** (CF_3) $>$ **6** (Cl) $>$ **7** (F) $>$ **4** (OMe) $>$ **3** (Me), which suggested that the presence of electron withdrawing *para* substituents favours higher activity. ^1H NMR spectra of the PCL indicated the presence of an BnO end group (*e.g.* Fig. S11, ESI[†]), which agrees with the MALDI-ToF mass spectra (*e.g.* Fig. S6, ESI[†]) and indicates that the polymerization proceeded *via* a coordination insertion mechanism. The observed molecular weights were lower than the calculated values, whilst the MALDI-ToF mass spectra were consistent with BnO end groups [$M = n \times 114.12$ (CL) + 108.05 (BnOH) + 22.99 (Na^+)]. In the absence of BnOH, spectra (Fig. S5 and S10, ESI[†]) indicated the products were catenulate with chains and cyclic polymers present. In the MALDI-ToF mass spectra, a part family of peaks consistent with the chain polymer (terminated by 2 OH) [$M = 17$ (OH) + 1(H) + $n \times 114.14$ (CL) + 22.99 (Na^+)] and the cyclic polymer [$M = 22.99$ (Na^+) + $n \times 114.14$ (CL)] were observed.

δ -Valerolactone (δ -VL)

Complexes **1–8** and **I–IV** were also evaluated as catalysts in the presence of one equivalent of BnOH for the ROP of



Table 2 ROP of ϵ -CL using 1–8 and I–IV in the presence of BnOH

Run	Cat.	CL : V : BnOH	<i>t</i> /h	<i>T</i> /°C	Conv ^a (%)	<i>M</i> _{n,GPC} × 10 ^{−3b}	<i>M</i> _w × 10 ^{−3b}	<i>M</i> _{n,Cal} × 10 ^{−3c}	PDI ^d	TON ^e	TOF ^f (h ^{−1})
1	1	1000 : 1 : 1	8	130	82.5	10.22	17.21	94.26	1.68	825	103
2	1	500 : 1 : 1	8	130	89.2	11.89	16.48	51.01	1.39	446	56
3	1	250 : 1 : 1	8	130	87.9	4.59	6.49	25.19	1.41	220	27
4	1	100 : 1 : 1	8	130	86.3	2.34	3.01	9.96	1.28	86	11
5	1	500 : 1 : 1	8	100	44.9	5.99	7.49	25.73	1.24	225	28
6	1	500 : 1 : 1	8	80	25.1	1.42	1.76	14.43	1.26	126	16
7	2	500 : 1 : 1	8	130	34.1	4.98	5.98	19.57	1.20	171	21
8	3	500 : 1 : 1	8	130	39.2	5.26	6.31	22.48	1.19	196	25
9	4	500 : 1 : 1	8	130	41.2	5.89	6.72	23.62	1.14	206	26
10	5	500 : 1 : 1	8	130	59.2	9.05	13.76	33.89	1.52	296	37
11	6	500 : 1 : 1	8	130	46.6	6.54	8.05	26.70	1.24	233	29
12	7	500 : 1 : 1	8	130	43.1	6.40	7.33	24.70	1.16	216	27
13	8	500 : 1 : 1	8	130	71.4	9.87	12.59	40.85	1.27	357	45
14	8	500 : 1 : 1	8	100	49.7	6.92	7.92	28.47	1.14	249	31
15	8	500 : 1 : 1	8	80	—	—	—	—	—	—	—
16	I	500 : 1 : 1	8	130	32.8	4.63	5.33	18.82	1.15	164	21
17	II	500 : 1 : 1	8	130	44.5	6.13	8.26	25.50	1.34	223	28
18	III	500 : 1 : 1	8	130	32.5	4.62	6.78	18.65	1.47	163	20
19	IV	500 : 1 : 1	8	130	30.8	2.76	3.12	17.68	1.12	154	19
20	1	500 : 1 : 1	24	130	99.4	11.61	16.42	56.83	1.41	497	21
21	2	500 : 1 : 1	24	130	65.3	5.56	7.42	37.37	1.33	327	14
22	3	500 : 1 : 1	24	130	90.3	5.20	6.42	51.63	1.23	452	19
23	4	500 : 1 : 1	24	130	96.5	6.13	7.51	55.17	1.23	483	20
24	5	500 : 1 : 1	24	130	99.0	9.52	11.01	56.60	1.16	495	21
25	6	500 : 1 : 1	24	130	98.1	7.45	8.53	56.08	1.14	491	20
26	7	500 : 1 : 1	24	130	98.3	7.12	8.56	56.20	1.20	492	20
27	8	500 : 1 : 1	24	130	99.5	10.33	13.63	56.88	1.32	498	21
28	I	500 : 1 : 1	24	130	62.5	4.36	7.63	35.77	1.75	313	13
29	II	500 : 1 : 1	24	130	76.2	6.88	7.52	43.59	1.09	381	16
30	III	500 : 1 : 1	24	130	60.5	5.12	6.23	34.63	1.22	303	13
31	IV	500 : 1 : 1	24	130	58.3	3.20	4.13	33.37	1.29	292	12

^a Determined by ¹H NMR spectroscopy. ^b *M*_{n,w}, GPC values corrected considering Mark–Houwink factor (0.56) from polystyrene standards in THF. ^c Calculated from ([monomer]₀/V) × conv (%) × monomer molecular weight (*M*_{CL} = 114.14) + molecular weight of BnOH. ^d From GPC. ^e Turnover number (TON) = number of moles of ϵ -CL consumed/number of moles V. ^f Turnover frequency (TOF) = TON/time (h).

Table 3 ROP of δ -VL using 1–8 and I–IV in the presence of BnOH

Run	Cat.	VL : V : BnOH	<i>t</i> /h	<i>T</i> /°C	Conv ^a (%)	<i>M</i> _{n,GPC} × 10 ^{−3b}	<i>M</i> _w × 10 ^{−3b}	<i>M</i> _{n,Cal} × 10 ^{−3c}	PDI ^d	TON ^e	TOF ^f (h ^{−1})
1	1	1000 : 1 : 1	8	130	79.9	10.57	18.69	80.10	1.76	799	100
2	1	500 : 1 : 1	8	130	86.3	12.38	16.31	43.31	1.31	432	54
3	1	250 : 1 : 1	8	130	84.6	4.26	6.45	21.28	1.51	212	26
4	1	100 : 1 : 1	8	130	82.1	2.38	3.95	8.33	1.70	82	10
5	1	500 : 1 : 1	8	100	42.1	6.01	7.22	21.18	1.20	211	26
6	1	500 : 1 : 1	8	80	20.5	1.89	3.25	10.37	1.72	103	13
7	2	500 : 1 : 1	8	130	35.9	4.28	6.51	18.08	1.52	180	22
8	3	500 : 1 : 1	8	130	38.4	5.23	7.24	19.33	1.38	192	24
9	4	500 : 1 : 1	8	130	44.3	6.90	8.49	22.28	1.23	222	28
10	5	500 : 1 : 1	8	130	58.1	9.43	13.25	29.19	1.40	291	36
11	6	500 : 1 : 1	8	130	43.9	6.27	7.53	22.08	1.20	220	27
12	7	500 : 1 : 1	8	130	42.1	5.94	7.56	21.18	1.27	211	26
13	8	500 : 1 : 1	8	130	75.5	10.61	14.64	37.90	1.38	378	47
14	I	500 : 1 : 1	8	130	37.0	4.84	5.47	18.63	1.12	185	23
15	II	500 : 1 : 1	8	130	48.9	7.24	8.92	24.59	1.23	245	31
16	III	500 : 1 : 1	8	130	35.6	4.21	6.21	17.93	1.48	178	22
17	IV	500 : 1 : 1	8	130	34.5	3.42	4.51	17.38	1.32	173	22

^a Determined by ¹H NMR spectroscopy. ^b *M*_{n,w}, GPC values corrected considering Mark–Houwink factor (0.57) from polystyrene standards in THF. ^c Calculated from ([monomer]₀/V) × conv (%) × monomer molecular weight (*M*_{VL} = 100.16) + molecular weight of BnOH. ^d From GPC. ^e Turnover number (TON) = number of moles of δ -VL consumed/number of moles V. ^f Turnover frequency (TOF) = TON/time (h).

δ -VL (Table 3). Using compound 1, the conditions of temperature and [V]: [δ -VL] were varied. Best observed results were achieved at 130 °C using [V]: [δ -VL] at 1:500

over 8 h. As in the case of the ROP of ϵ -CL, kinetic studies (Fig. 7 and S3, ESI†) revealed that the catalytic activities followed the order: 1 > 8 > II > I > III ≈ 3 > 2 > IV,



Table 4 ROP of co-polymer (ϵ -CL + δ -VL) using **1–8** and **I–IV** in the presence of BnOH

Run	Cat	CL:VL:V:BnOH	$T/^\circ\text{C}$	CL:VL ^a	Conv ^b (%)	$M_{n,\text{GPC}} \times 10^{-3c}$	$M_w \times 10^{-3c}$	PDI ^d
1	1 ^e	250:250:1:1	130	45:55	72.6	12.16	22.37	1.84
3	2 ^e	250:250:1:1	130	45:55	25.3	1.32	2.31	1.75
4	3 ^e	250:250:1:1	130	40:60	45.2	4.68	6.23	1.33
5	4 ^e	250:250:1:1	130	33:67	47.5	5.29	6.88	1.30
6	5 ^e	250:250:1:1	130	40:60	59.5	7.21	8.45	1.17
7	5 ^f	250:250:1:1	130	66:34	63.7	7.44	8.95	1.20
8	5 ^g	250:250:1:1	130	58:42	35.8	4.22	7.12	1.69
9	6 ^e	250:250:1:1	130	40:60	57.9	6.01	7.52	1.25
10	6 ^f	250:250:1:1	130	62:38	55.4	6.21	7.69	1.24
11	6 ^g	250:250:1:1	130	50:50	38.5	5.98	8.15	1.36
12	7 ^e	250:250:1:1	130	50:50	58.4	6.12	7.14	1.17
13	8 ^e	250:250:1:1	130	51:49	60.8	6.85	8.69	1.27
15	I ^e	250:250:1:1	130	46:54	61.1	6.95	8.69	1.25
16	II ^e	250:250:1:1	130	45:55	58.1	3.67	4.98	1.36
17	III ^e	250:250:1:1	130	40:60	49.5	4.53	7.21	1.59
18	IV ^e	250:250:1:1	130	35:65	38.4	4.21	6.49	1.54

^a Ratio of ϵ -CL to δ -VL observed in the co-polymer by ^1H NMR spectroscopy. ^b Determined by ^1H NMR spectroscopy. ^c $M_{n/w}$, GPC values corrected considering Mark-Houwink method from polystyrene standards in THF, $M_{n/w} \text{ GPC} = [0.56 \times M_{n/w} \text{ measured} \times (1\% \text{ CL}) + 0.57 \times M_{n/w} \text{ measured} \times (1\% \text{ VL})] \times 10^3$. ^d From GPC. ^e ϵ -Caprolactone was firstly added for 24 h, then δ -valerolactone was added and heating for 24 h. ^f δ -Valerolactone was firstly added for 24 h, then ϵ -caprolactone was added and heating for 24 h. ^g ϵ -Caprolactone and δ -valerolactone were added at the same time and heating for 24 h.

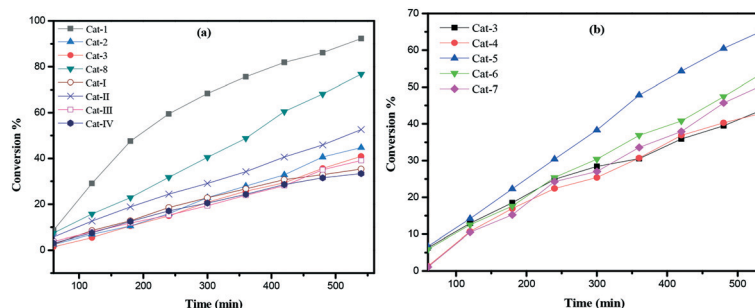


Fig. 6 (a) Relationship between conversion and time for the polymerization of ϵ -CL by using complex **1–3**, **8**, and **I–IV**; (b) relationship between conversion and time for the polymerization of ϵ -CL by using complexes **3–7**; conditions: $T = 130^\circ\text{C}$, $n_{\text{Monomer}}: n_{\text{V}}: \text{BnOH} = 500:1:1$.

whilst the performance of the vanadium-based imido catalysts exhibited the order $5 > 6 \approx 7 > 4 > 3$, which was again suggestive of a positive influence exerted by electron-withdrawing *para* substituents on the imido group. As for the ROP of ϵ -CL, there was evidence of significant transesterification and nearly all observed M_n values were

significantly lower than the calculated values. The MALDI-ToF mass spectra (Fig. S8, ESI†) exhibited a major family of peaks consistent with OBn end groups [$M = 108.05$ (BnOH) + $n \times 100.12$ (VL) + 22.99 (Na^+)], and a minor family assigned to cyclic PVL. ^1H NMR spectra of the PVL also indicated the presence of an BnO end group (e.g. Fig. S13,

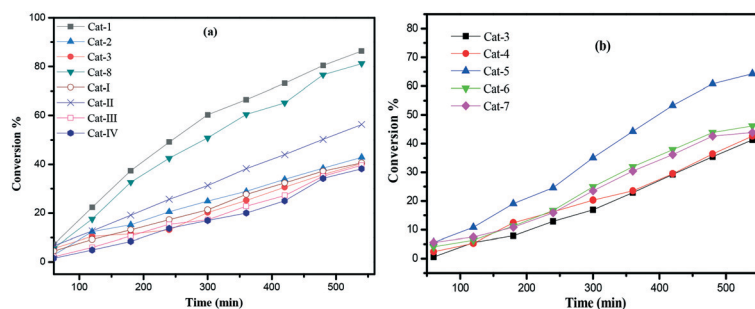


Fig. 7 (a) Relationship between conversion and time for the polymerization of δ -VL by using **1–3**, **8**, and **I–IV**; (b): Relationship between conversion and time for the polymerization of δ -VL by using complexes **3–7**; conditions: $T = 130^\circ\text{C}$, $n_{\text{Monomer}}: n_{\text{V}}: \text{BnOH} = 500:1:1$.



ESI[†]). In the absence of BnOH, spectra (Fig. S7 and S12, ESI[†]) again indicated the products were catenulate. The MALDI-ToF mass spectra exhibited the peaks consistent with the chain polymer (terminated by 2 OH) [$M = 17(\text{OH}) + 1(\text{H}) + n \times 100.12(\text{VL}) + 22.99(\text{Na}^+)$] and cyclic polymer [$M = 22.99(\text{Na}^+) + n \times 100.12(\text{VL})$].

Kinetics

The kinetic results are consistent with a zero-order dependence in monomer. Whilst this kind of behaviour is uncommon, systems that behave in a similar manner have been reported.¹⁹ The dependence of the M_n and molecular weight distribution on the monomer conversion in the reactions catalyzed by **1**, **3** and **8** with BnOH was also investigated (Fig. 8). For the ROP of ϵ -CL, the M_n was shown to increase linearly with the conversion, which suggested that the polymerization was well controlled (Fig. 8, left). A similar outcome was also observed in the reaction involving δ -VL (Fig. 8, right).

Co-polymerization of ϵ -CL and δ -VL

The complexes exhibited moderate conversions, with the mixed-metal complex **1** performing best (72.6%), with **5** ($p\text{-CF}_3$) and the known complex **I** also producing conversions >60%. Under the conditions employed, the systems **5**, **6**, **7** and **8** showed a preference for CL incorporation (50–66%), and in the case of **5** and **6**, this was despite the initial addition of δ -VL. Complex **4** exhibited the highest preference (67%) for VL incorporation. In general, the systems appeared to be relatively well behaved with PDIs in the range 1.17–1.84; NMR spectra were consistent with the presence of BnO and OH end groups (Fig. S15, ESI[†]). The composition of the copolymer was further investigated by ^{13}C NMR spectroscopy. In fact, diagnostic resonances belonging to CL–VL, CL–CL, VL–VL and VL–CL dyads can be observed in the region between δ 63.91 and 64.13 ppm (Fig. 16, ESI[†]). Based on the current results, the number-average sequence length was found to be 7.16 and 5.30 for CL and VL, respectively, consistent with a randomness degree R of 0.33, which suggests the copolymers possess a “blocking” tendency (Fig. S16, eqn (S1)–(S3), ESI[†]).²⁰

ROP of r -lactide

To enhance the thermal properties of the polymers obtained herein, we also investigated the ROP of the r -lactide. Unfortunately, none of the systems herein proved to be effective as catalysts for the ROP of r -lactide either in solution at high temperatures (130 °C) or as melts.

Ethylene polymerization

The imido complexes **3**–**7** were screened for their ability to polymerize ethylene in the presence of the co-catalysts R_2AlCl ($\text{R} = \text{Me}, \text{Et}$) and the re-activator ethyltrichloroacetate (ETA), see Table 5, showing much higher polymerization activities if Me_2AlCl was used as activator (*cf.* entries 1 and 2 of Table 5). In the presence of $\text{Me}_2\text{AlCl} + \text{ETA}$, the catalytic activities followed the trend **3** ($p\text{-Me}$) \approx **5** ($p\text{-CF}_3$) > **7** ($p\text{-F}$) > **6** ($p\text{-Cl}$) > **4** ($p\text{-OMe}$). Complexes **3**–**7** exhibited high ethylene consumption rates during 10–20 min of polymerization and virtually lost the activity after 30 min (Fig. 9a). Complex **4** showed the lowest reactivity toward ethylene in the series, which may be explained by the presence of strong electron-donating OMe substituents, reducing its electrophilicity. All systems except **4** were relatively well-controlled with PDIs < 2.5 (Fig. 9b) and afforded highly linear (according to ^{13}C NMR spectroscopy, there were no detectable branches, Fig. S25, ESI[†]) high molecular weight polyethylene. The ethylene polymerization activities found here for complexes **3**–**7**, are very high, several times higher than those reported for vanadium polyphenolate and phenoxyimine catalysts under comparable conditions.²¹

Conclusions

In conclusion, the use of $p\text{-tert-butyltetrahomodioxacalix[6]}$ arene H_6 , L^6H_6 , with $[\text{NaVO}(\text{OtBu})_4]$ or $[\text{VO}(\text{OnPr})_3]$ affords the mixed-metal complex $[(\text{VO})_2(\mu\text{-O})\text{Na}_2(\text{L}^1)(\text{MeCN})_4]$ or the tetranuclear complex $\{[\text{VO}]_4\text{L}^1\}$, respectively. Use of imido-alkoxide precursors $[\text{V}(\text{Np-RC}_6\text{H}_4)(\text{OR})_3]$ leads to the formation of $\{[\text{V}(\text{Np-RC}_6\text{H}_4)]_2\text{L}^1\}$ type complexes. Under the conditions employed, the calixarene ring system can break *in situ*, and result in two 2-($p\text{-CH}_3\text{C}_6\text{H}_4\text{NCH}$)-4- $t\text{Bu-C}_6\text{H}_2\text{O-6-CH}_2$)-4- $t\text{BuC}_6\text{H}_2\text{OH}$ (L^2), which can bind to the vanadium to form a metallocyclic complex of the form $[\text{VO}(\text{L}^2)]_2$. All

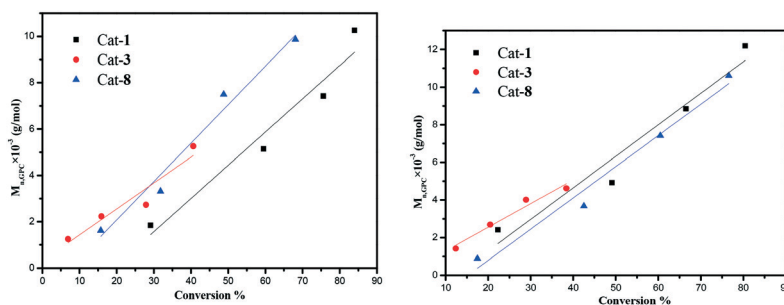


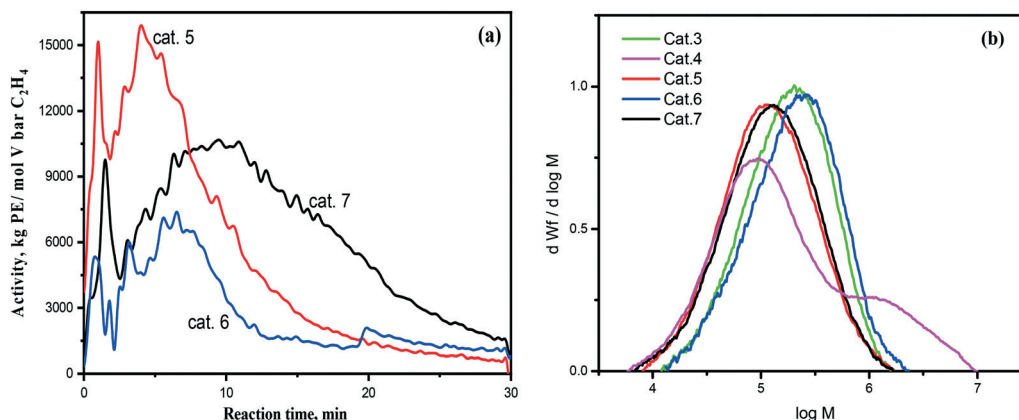
Fig. 8 Left: M_n vs. monomer conversion in the ROP of ϵ -CL by using **1**, **3** and **8**; right: M_n vs. monomer conversion in the ROP of δ -VL by using **3** and **8**; conditions: $T = 130^\circ\text{C}$, $n_{\text{Monomer}}:n_{\text{V}}: \text{BnOH} = 500:1:1$.



Table 5 Ethylene polymerization data for homogeneous catalysts (R-Ph-LV₂ + Me₂AlCl + ETA)

Run	Cat	V loading/ μmol	Co-catalyst	PE yield/g	Activity ^a	$M_n \times 10^{-3}$	$M_w \times 10^{-3}$	M_z/M_w	PDI ^b
1	3	1.0	Et ₂ AlCl	0.7	1.4	—	—	—	—
2	3	0.5	Me ₂ AlCl	7.4	14.8	110	245	1.8	2.2
3	4	0.5	Me ₂ AlCl	1.2	2.4	72	520	5.0	7.2
4	5	0.5	Me ₂ AlCl	7.2	14.2	74	180	2.1	2.4
5	6	0.5	Me ₂ AlCl	4.5	9.0	120	290	1.9	2.4
6	7	0.5	Me ₂ AlCl	6.7	13.4	74	185	2.0	2.5

^a In 10^6 g PE mol V⁻¹ bar⁻¹ h⁻¹. ^b PDI = M_w/M_n .

**Fig. 9** (a) Activity vs. time plot for entries 4–6 of Table 5. (b) GPC traces of polyethylenes in entries 2 and 4–6 of Table 5.

complexes were active for the ROP of the cyclic esters ϵ -CL and δ -VL, with and without benzyl alcohol (BnOH) present, but not for *r*-LA. The co-polymerization of ϵ -CL with δ -VL was also possible. Low molecular weight products were obtained but with good control. For the imido complexes in the presence of BnOH, kinetic studies indicated the rate order 5 (CF₃) > 6 (Cl) > 7 (F) > 4 (OMe) > 3 (Me) for ϵ -CL which suggested that the presence of electron withdrawing *para* substituents favour higher activity, and a similar order for δ -VL; in the absence of BnOH, structure/activity trends were less evident. Observed conversion rates were superior to related oxacalix[3]arene species (**I** and **II**) as well as methylene (–CH₂–) bridged calix[6 and 8]arene complexes **III** and **IV** under similar conditions. This suggests the presence and large flexibility of the dioxacalix[6]arene scaffold is beneficial in ROP. For ethylene polymerization (with DMAC/ETA), the imido complexes **3** and **5–7** showed very high catalytic activities of the order $0.9\text{--}1.5 \times 10^7$ g PE (mol V)⁻¹ bar⁻¹ h⁻¹, which followed the trend 3 (*p*-Me) \approx 5 (*p*-CF₃) > 7 (*p*-F) > 6 (*p*-Cl), whilst the activity of **4** (*p*-OMe) was much lower and was thought to be due to its reduced electrophilicity. The product in each case was highly linear polyethylene.

Experimental

General

The known compounds L¹H₆, L³H₃, [V(Np-RC₆H₄)(OiPr)₃] (R = OMe, CF₃, Cl), [V(Np-CH₃C₆H₄)(OtBu)₃] and [V(Np-CH₃C₆H₄)

(OEt)₃], [VOL³] (L³ = oxacalix[3]arene) (**I**), [V(Np-CH₃C₆H₄)L³]₂ (**II**), [Li(MeCN)₄][V₂(O)₂Li(MeCN)(L⁶H₆)₂] (L⁶H₆ = *p*-*tert*-butylcalix[6]areneH₆) (**III**), [(VO)₂L⁸H₈] (L⁸H₈ = *p*-*tert*-butylcalix[8]areneH₈) (**IV**) and [VOL⁴] (L⁴ = 2,6-bis(3,5-*tert*-butyl-2-hydroxybenzyl)-4-*tert*-butylphenol) (**V**) were prepared by the literature methods.^{7,9,15,16,22} All reactions were conducted under an inert atmosphere using standard Schlenk techniques. Toluene was dried from sodium, acetonitrile was distilled from calcium hydride, diethylether was distilled from sodium benzophenone, and all solvents were degassed prior to use. IR spectra (nujol mulls, KBr or NaCl windows) were recorded on a Nicolet Avatar 360 FT IR spectrometer.

¹H NMR spectra were recorded at room temperature on a Varian VXR 400 S spectrometer at 400 MHz or a Gemini 300 NMR spectrometer or a Bruker Avance DPX-300 spectrometer at 300 MHz. ¹H and ¹³C NMR spectra of polyethylene samples (1,2-dichlorobenzene, 100 °C) were recorded on a Bruker Avance 400 MHz NMR spectrometer at 400.130 and 100.613 MHz, respectively. ¹H NMR spectra were calibrated against the residual protio impurity of the deuterated solvent.

Crystal structures were determined from data collected at the UK National Crystallography Service (**1–6**) and the SRS at Daresbury (**8**). Full details are given in the ESI.† Crystal data are summarised in Table 6.

Elemental analyses were performed by the elemental analysis service at the University of Hull. Matrix assisted laser desorption/ionization time of flight (MALDI-TOF) mass spectrometry was performed in a Bruker autoflex III smart



beam in linear mode, and the spectra were acquired by averaging at least 100 laser shots. 2,5-Dihydroxybenzoic acid was used as the matrix and THF as solvent. Sodium chloride was dissolved in methanol and used as the ionizing agent. Samples were prepared by mixing 20 μL of matrix solution in THF (2 mg mL^{-1}) with 20 μL of matrix solution (10 mg mL^{-1}) and 1 μL of a solution of ionizing agent (1 mg mL^{-1}). Then 1 mL of these mixtures was deposited on a target plate and allowed to dry in air at ambient temperature.

Weight-average (M_w) and number-average (M_n) molecular weights, molecular weight distributions (MWD), and polydispersities (M_w/M_n) were measured on a waters-150 chromatograph at 150 $^{\circ}\text{C}$, with trichlorobenzene as solvent.

Preparation of $[(\text{VO})_2(\mu\text{-O})\text{Na}_2(\text{L}^1)(\text{MeCN})_4]\cdot 5\text{MeCN}$ (1.5MeCN)

To *in situ* $\text{Na}[\text{VO}(\text{OtBu})_4]$ (generated from 0.98 mmol from VOCl_3 and 4tBuONa) in Et_2O (30 mL) was added L^1H_6 (0.50 g, 0.49 mmol) and at $-78\text{ }^{\circ}\text{C}$. The mixture was allowed to warm to ambient temperature and then the volatiles were removed *in vacuo*. Toluene (30 mL) was then added and the system was refluxed for 12 h. On cooling, volatiles were removed *in vacuo*, and the residue was extracted into warm MeCN (30 mL). On prolonged standing at 0 $^{\circ}\text{C}$, green prisms of **1** formed. Yield 0.46 g, 34%. Anal. calcd for $\text{C}_{86}\text{H}_{109}\text{N}_9\text{Na}_2\text{O}_{11}\text{V}_2$: C, 64.85; H, 6.90; N 7.92%; found C, 65.22; H, 7.5%; 7.23%. IR (nujol mull, KBr): 3901w, 3422w, 1747w, 1260s, 1227w, 1199m, 1059s, 1021s, 965m, 903w, 868m, 831w, 796s, 708w, 658m, 641m, 623m, 602w, 553w, 453w. ^1H NMR (CDCl_3) δ : 8.00–7.5 (m, 12H, arylH), 5.71 (d, $J = 8.1$, 4H, $-\text{OCH}_2$), 4.90 (d, $J = 8.1$, 4H, OCH_2), 4.05 (d, $J = 8.0$, 4H, $-\text{CH}_2$), 3.53 (d, $J = 8.0$, 4H, $-\text{CH}_2$), 2.05 (s, CH_3CN), 1.35–1.24 (m, 54H, $\text{C}(\text{CH}_3)_3$). ^{51}V NMR (CDCl_3) δ : -675.3 ppm ($\omega_{1/2}$ 272 Hz). Mass spec (EI): 1592 $[\text{M}]^+$.

Synthesis of $[(\text{VO})_4\text{L}^1]$ (2.6MeCN)

$[\text{VO}(\text{OnPr})_3]$ (0.49 g, 2.0 mmol) and L^1H_6 (0.50 g, 0.49 mmol) were combined in toluene (20 mL). After refluxing for 12 h, volatiles were removed *in vacuo*, and the residue was extracted into MeCN (20 mL). Prolonged standing at 0 $^{\circ}\text{C}$ afforded 2.6MeCN as dark blue prisms. Yield 0.32 g, 49%. Anal. calcd for $\text{C}_{74}\text{H}_{96}\text{O}_{16}\text{V}_4$ (sample dried *in vacuo* for 12 h): C, 61.49; H, 6.70%. Found C, 61.49; H, 6.53%. IR (nujol mull, KBr): 1651w, 1599m, 1461s, 1377s, 1363m, 1304w, 1260s, 1206m, 1092s, 1052s, 1016s, 986m, 922w, 873m, 851m, 799 s. ^1H NMR (CDCl_3) δ : 6.88–7.35 (m, 12H, arylH), 6.07 (d, $J = 4.8$ Hz, 2H, $-\text{OCH}_2$), 5.77 (m, 2H, $-\text{OCH}_2$), 5.51 (d, $J = 4.8$ Hz, 2H, $-\text{OCH}_2$), 5.15 (m, 4H, $-\text{OCH}_2\text{CH}_2\text{CH}_3$), 4.86 (d, $J = 4.8$ Hz, 2H, $-\text{OCH}_2$), 4.20 (m, 4H, $-\text{CH}_2$), 3.40 (d, $J = 12.4$ Hz, 4H, $-\text{CH}_2$), 2.32 (m, 4H, $-\text{OCH}_2\text{CH}_2\text{CH}_3$), 1.13–1.49 (m, 54H, $\text{C}(\text{CH}_3)_3$), 1.02 (m, 6H, $-\text{OCH}_2\text{CH}_2\text{CH}_3$). ^{51}V NMR (CDCl_3) δ : -411.7 ($\omega_{1/2}$ 524 Hz), -461.5 ppm ($\omega_{1/2}$ 735 Hz). Mass spec (EI): 1351 $[\text{M} + \text{Na} - 2\text{OnPr}]^+$.

Preparation of $[\text{V}(\text{Np}-\text{CH}_3\text{C}_6\text{H}_4)]_2\text{L}^1$ (3.7MeCN-0.5 CH_2Cl_2)

To $[\text{V}(\text{Np}-\text{CH}_3\text{C}_6\text{H}_4)(\text{OtBu})_3]$ (0.37 g, 0.99 mmol) and L^1H_6 (0.50 g, 0.49 mmol) was added toluene (30 mL) and then the

system was refluxed for 12 h. On cooling, the volatiles were removed *in vacuo*, and the residue was extracted into warm MeCN (30 mL). On prolonged standing at 0 $^{\circ}\text{C}$, an orange crystalline material formed, yield 0.61 g, 47%. Single orange prisms of 3.7MeCN-0.5 CH_2Cl_2 were grown from a saturated MeCN solution containing CH_2Cl_2 (2 mL) at 0 $^{\circ}\text{C}$. Anal. calcd for $\text{C}_{82}\text{H}_{96}\text{N}_2\text{O}_8\text{V}_2$: C, 73.41; H, 7.21; N, 2.12%; found C, 73.32%; H, 7.41%, N, 2.24%. IR (nujol mull, KBr): 3236w, 2727w, 2349w, 2288w, 2248w, 1614m, 1592m, 1556w, 1300m, 1261s, 1073s, 1020s, 990m, 937m, 878m, 840s, 819s, 763s, 754w, 722w, 696w, 639w, 584w. ^1H NMR (CDCl_3) δ : 7.78–6.85 (m, 12H, aryl-H), 6.46 (d, $J = 8.4$ Hz, 4H, $-\text{N}-\text{C}_6\text{H}_4-$), 6.16 (d, $J = 8.4$ Hz, 4H, $-\text{N}-\text{C}_6\text{H}_4-$), 4.86–5.10 (d, $J = 7.6$ Hz, 4H, OCH_2), 4.53–4.66 (m, 4H, $-\text{OCH}_2$), 4.34–4.25 (m, 4H, $-\text{CH}_2$) 3.66–4.00 (d, $J = 12.4$ Hz, 4H, $-\text{CH}_2$), 2.35 (m, 6H, *p*-tolyl- CH_3), 2.05 (s, 3H, MeCN) 1.49 (m, 54H, $\text{C}(\text{CH}_3)_3$). ^{51}V NMR (CDCl_3) δ : -312.2 ($\omega_{1/2}$ 650 Hz) ppm. Mass spec (EI): 1362 $[\text{M} + \text{Na}]^+$, 1379 $[\text{M} + \text{K}]^+$.

Synthesis of $[\text{V}(\text{Np}-(\text{OMe})\text{C}_6\text{H}_4)]_2\text{L}^1$ (4.4MeCN)

As for **2**, but using $[\text{V}(\text{Np}-(\text{OMe})\text{C}_6\text{H}_4)(\text{OiPr})_3]$ (0.35 g, 1.0 mmol) and L^1H_6 (0.50 g, 0.49 mmol) affording 4.4MeCN as orange/red prisms. Single orange prisms were grown from a saturated MeCN (30 mL) solution at 0 $^{\circ}\text{C}$; yield 0.43 g, 50%. Anal. calcd for $\text{C}_{82}\text{H}_{96}\text{N}_2\text{O}_{10}\text{V}_2$ (sample dried *in vacuo* for 12 h): C, 71.80; H, 7.06; N, 2.04%. Found C, 71.78; H, 7.14; N, 2.38%. IR (nujol mull, KBr): 3237w, 1613w, 1585m, 1554w, 1540w, 1486m, 1459s, 1383m, 1362w, 1297w, 1260s, 1206m, 1159 m 1075s, 1023s, 910w, 872m, 800s, 754w, 688m. ^1H NMR (CDCl_3) δ : 6.87–7.54 (m, 12H, arylH), 6.49 (d, $J = 8.0$ Hz, 4H, $-\text{NC}_6\text{H}_4-\text{OMe}$), 5.88 (d, $J = 8.0$ Hz, 4H, $-\text{NC}_6\text{H}_4-\text{OMe}$), 5.11 (d, $J = 6.8$ Hz, 4H, $-\text{OCH}_2$), 4.95 (d, $J = 6.8$ Hz, 4H, $-\text{OCH}_2$), 4.47–4.67 (m, 4H, $-\text{CH}_2$), 3.64 (d, $J = 5.2$ Hz, 4H, $-\text{CH}_2$), 3.51 (s, 6H, *p*- $\text{C}_6\text{H}_4-\text{OCH}_3$), 2.01 (s, 3H, MeCN), 1.35–1.15 (m, 54H, $\text{C}(\text{CH}_3)_3$). ^{51}V NMR (CDCl_3) δ : -178.1 ($\omega_{1/2}$ 470 Hz) ppm. Mass spec (EI): 1470 $[\text{M} + \text{Na}]^+$.

Synthesis of $[\text{V}(\text{Np}-(\text{CF}_3)\text{C}_6\text{H}_4)]_2\text{L}^1$ (5)

As for **2**, but using $[\text{V}(\text{Np}-(\text{CF}_3)\text{C}_6\text{H}_4)(\text{OiPr})_3]$ (0.38 g, 1.0 mmol) and L^1H_6 (0.50 g, 0.49 mmol) affording **5** as orange/brown prisms. Single orange prisms were grown from a saturated MeCN (30 mL) solution at 0 $^{\circ}\text{C}$ (yield 0.26 g, 36%). Anal. Calcd for $\text{C}_{82}\text{H}_{90}\text{F}_6\text{N}_2\text{O}_8\text{V}_2$: C, 68.04; H, 6.27; N, 1.94%. Found: C, 67.36; H, 6.45; N, 2.32%. IR (nujol mull, KBr): 1730w, 1598m, 1557m, 1509m, 1456s, 1383s, 1363w, 1324s, 1260s, 1201w, 1163m, 1059s, 1067s, 1071s, 956w, 877m, 849m, 799s, 723 m. ^1H NMR (CDCl_3) δ : 6.84–7.82 (m, 12H, arylH), 6.51 (d, $J = 8.8$ Hz, 4H, $-\text{C}_6\text{H}_4-\text{CF}_3$), 6.19 (m, 4H, $-\text{C}_6\text{H}_4-\text{CF}_3$), 5.02–4.91 (m, 4H, $-\text{OCH}_2$), 4.52 (d, $J = 5.2$ Hz, 4H, $-\text{OCH}_2$), 4.27–4.16 (m, 4H, $-\text{CH}_2$), 3.72 (m, 4H, $-\text{CH}_2$), 1.95 (s, 3H, MeCN), 1.35–1.06 (m, 54H, $\text{C}(\text{CH}_3)_3$). ^{51}V NMR (CDCl_3) δ : -408.1 ppm ($\omega_{1/2}$ 474 Hz). ^{19}F NMR (CDCl_3) δ : -62.69 ppm. Mass spec (EI): 1441 $[\text{M}]$.

Synthesis of $[\text{V}(\text{Np}-\text{Cl}-\text{C}_6\text{H}_4)]_2\text{L}^1$ (6)

As for **2**, but using $[\text{V}(\text{Np}-\text{Cl}-\text{C}_6\text{H}_4)(\text{OiPr})_3]$ (0.35 g, 1.0 mmol) and L^1H_6 (0.50 g, 0.49 mmol) affording **6** as dark brown



prisms from a saturated MeCN (30 mL) solution at 0 °C (yield 0.35 g, 51%). Anal. calcd for $C_{80}H_{90}Cl_2N_2O_8V_2 \cdot MeCN$ C, 69.29; H, 6.89; N, 2.96%. Found C, 67.72; H, 7.43; N 2.25%.²³ IR (nujol mull, KBr): 2359m, 1737w, 1593m, 1554m, 1513m, 1461s, 1377m, 1294m, 1260m, 1200 m, 1117s, 1088w, 822w, 795w, 726w. ¹H NMR (CDCl₃) δ : 6.88–7.69 (m, 12H, arylH), 6.50 (d, J = 10.0 Hz, 4H, $-C_6H_4-Cl$), 6.35 (d, J = 10.0 Hz, 4H, $-C_6H_4-Cl$), 4.86–5.09 (m, J = 10.0 Hz, 4H, $-OCH_2-$), 4.68 (d, J = 10.0 Hz, 4H, $-OCH_2-$), 4.31–4.53 (m, 4H, $-CH_2-$), 3.67 (d, J = 12.8 Hz, 4H, $-CH_2-$), 1.13–1.35 (m, 54H, $C(CH_3)_3$). ⁵¹V NMR (CDCl₃) δ : –335.3 ppm ($\omega_{1/2}$ 120 Hz). Mass spec (EI): 1386 [M]⁺.

Synthesis of $\{[V(Np-F-C_6H_4)]_2L^1\}$ (7-MeCN)

As for 2, but using $[V(Np-F-C_6H_4)(OnPr)_3]$ (0.34 g, 0.99 mmol) and L^1H_6 (0.50 g, 0.49 mmol) affording 7-MeCN as red/brown crystals from a saturated MeCN (30 mL) solution at 0 °C. Yield: 0.57 g, 86%. Anal. calcd for $C_{80}H_{90}F_2N_2O_8V_2 \cdot MeCN$ C, 70.92; H, 6.75; N, 3.03%. Found C, 70.72; H, 6.89; N 3.38%. IR (nujol mull, KBr): 2360w, 2341w, 1682w, 1510 m, 1411w, 1299w, 1260s, 1228m, 1202s, 1155w, 1144w, 1096s, 1064s, 1017s, 988m, 912w, 872w, 832s, 821s, 806s, 722m, 668w, 581w, 460w. ¹H NMR (CDCl₃) δ : 6.84–7.81 (m, 12H, arylH), 6.49 (d, J = 6.8 Hz, 4H, $-NC_6H_4-Cl$), 5.91 (d, J = 6.8 Hz, 4H, $-NC_6H_4-Cl$), 4.91–4.98 (d, J = 8.8 Hz, 4H, $-OCH_2-$), 4.49 (d, J = 8.8 Hz, 4H, $-OCH_2-$), 4.13–4.26 (m, 4H, $-CH_2-$), 3.69 (d, J = 5.2 Hz, 4H, $-CH_2-$), 1.36–1.09 (m, 54H, $C(CH_3)_3$). ¹⁹F NMR (CDCl₃) δ : 108.30 ppm. ⁵¹V NMR (CDCl₃) δ : –173.4 ppm ($\omega_{1/2}$ 265 Hz).

Synthesis of $[VO(L^2)]_2$ (L^2 = 2-(*p*-tolylNCH)-4-*t*Bu-C₆H₂O-6-CH₂)-4-*t*Bu-C₆H₂OH) (8·4MeCN)

$[V(Np-tolyl)(OEt)_3]$ (0.29 g, 0.99 mmol) and L^1H_6 (0.50 g, 0.49 mmol) were refluxed in toluene (30 mL) for 12 h. Following removal of volatiles *in vacuo*, the residue was dissolved in hot MeCN (30 mL), filtered and left to stand (1–2 days) at 0 °C to afford 8 as orange-brown prisms (0.43 g, 29% yield). Anal. calcd for $C_{96}H_{108}N_4O_8V_2$ (sample dried *in vacuo* for 12 h, $-4MeCN$): C, 74.49; H, 7.03; N 3.62%; found C, 73.60; H, 7.12; N, 2.88%. IR (nujol mull, KBr): 3231w, 1613m, 1593m, 1555w, 1505w, 1459s, 1377s, 1363m, 1299w, 1261s, 1209s, 1073s, 1019s, 991, 965m, 878s, 871s, 839m, 818m, 802s, 765w, 764m, 753 m, 737m. ¹H NMR (CDCl₃) results of complex 7. ¹H NMR (CDCl₃) δ : 9.01 (s, 2H, $-OH$), 6.84–7.68 (m, 12H, arylH), 6.45 (d, J = 8.4 Hz, 4H, $-NC_6H_4-Me$), 6.16 (d, J = 8.4 Hz, 4H, $-NC_6H_4-Me$), 4.85–5.10 (d, J = 9.6 Hz, 4H, $-N-CH_2-$), 4.53–4.65 (d, J = 9.6 Hz, 4H, $-N-CH_2-$), 4.25–4.34 (m, 4H, $-CH_2-$), 3.65 (d, J = 12.8 Hz, 4H, $-CH_2-$), 2.33 (m, 12H, $-CH_3$), 2.01 (s, 3H, MeCN), 1.11–1.36 (m, 54H, $C(CH_3)_3$). ⁵¹V NMR (CDCl₃) δ : –513.2 ppm ($\omega_{1/2}$ 512 Hz). Mass spec (EI): 1556 [M + Na⁺–3MeCN].

Procedure for ROP of ϵ -caprolactone/ δ -valerolactone

A toluene solution of pre-catalyst (0.010 mmol, 1.0 mL toluene) was added into a Schlenk tube in the glove-box at room temperature. The solution was stirred for 2 min, and

then the appropriate equivalent of BnOH (from a pre-prepared stock solution of 1 mmol BnOH in 100 mL toluene) and the appropriate amount of ϵ -CL or δ -VL along with 1.5 mL toluene was added to the solution. For example, for Table 2, entry 1, a toluene solution of pre-catalyst 1 (0.010 mmol, 1.0 mL toluene) was added into a Schlenk tube, then 2 mL BnOH solution (1 mmol BnOH/100 mL toluene) and 20 mmol ϵ -CL along with 1.5 mL toluene was added to the solution. The reaction mixture was then placed into an oil/sand bath pre-heated at 130 °C, and the solution was stirred for the prescribed time (8 or 24 h). The polymerization mixture was quenched on addition of an excess of glacial acetic acid (0.2 mL) into the solution, and the resultant solution was then poured into methanol (200 mL). The resultant polymer was then collected on filter paper and was dried *in vacuo*.

Kinetic studies

The polymerizations were carried out at 130 °C in toluene (2 mL) using 0.010 mmol of complex. The molar ratio of monomer to initiator was fixed at 500:1, and at appropriate time intervals, 0.5 μ L aliquots were removed (under N₂) and were quenched with wet CDCl₃. The percent conversion of monomer to polymer was determined using ¹H NMR spectroscopy.

Procedure for ethylene polymerization

Ethylene polymerization experiments were performed in a steel 500 mL autoclave. The reactor was evacuated at 80 °C, cooled down to 20 °C and then charged with the freshly prepared solution of the co-catalyst in heptane/toluene. Pre-catalysts were introduced into the reactor in sealed glass ampoules, containing 0.5 or 1.0 μ mol of appropriate V-complex in 0.5 mL of solvent. After setting up the desired temperature and ethylene pressure, the reaction was started by breaking the ampoule with the pre-catalyst. During the polymerization, ethylene pressure (2 bar), temperature (70 °C) and stirring speed (2000 rpm) were maintained constant. After 30 min (during which time the ethylene consumption rate declined to nearly zero level), the reactor was opened to the atmosphere and the polymeric product was dried in a fume-hood to a constant weight.

Polymerization conditions. For entry 1 of Table 5: V loading 1.0 μ mol (dissolved in CH₂Cl₂), co-catalyst Et₂AlCl + ETA (molar ratio V:Et₂AlCl:ETA = 1:1000:500) in 50 mL of toluene + 100 mL of heptane, T_{pol} 70 °C, $P_{C_2H_4}$ = 2 bar, for 30 min. For entries 2–8 of Table 5: V complex was dissolved in toluene, Co-catalyst Me₂AlCl + ETA (molar ratio V:Me₂AlCl:ETA = 1:1000:1000) in 100 mL of toluene + 100 mL of heptane; T_{pol} 70 °C, $P_{C_2H_4}$ = 2 bar, for 30 min.

Crystallography



Table 6 Crystal structure data for 1-5MeCN, 2-6MeCN, 3-7MeCN-0.5CH₂Cl₂, 4-4MeCN, 5, 6, 7, 8-4MeCN^{a,b}, (ref. 24)

Compound	1-5MeCN	2-6MeCN	3-7MeCN-0.5CH ₂ Cl ₂	4-4MeCN
Formula	C ₈₆ H ₁₀₉ N ₉ Na ₂ O ₁₁ V ₂	C ₈₆ H ₁₁₄ N ₆ O ₁₆ V ₄	C ₃₅₅ H ₄₂₁ Cl ₂ N ₂₁ O ₃₂ V ₈	C ₉₀ H ₁₀₈ N ₆ O ₁₀ V ₂
Formula weight	1592.68	1691.59	5972.52	1535.77
Crystal system	Triclinic	Triclinic	Triclinic	Triclinic
Space group	<i>P</i> $\bar{1}$	<i>P</i> $\bar{1}$	<i>P</i> $\bar{1}$	<i>P</i> $\bar{1}$
Unit cell dimensions				
<i>a</i> (Å)	13.4214(3)	12.4983(4)	19.7899(3)	14.03537(8)
<i>b</i> (Å)	14.2596(5)	13.6976(2)	20.6775(3)	17.33956(12)
<i>c</i> (Å)	25.2549(7)	14.1554(3)	22.7696(5)	20.19059(12)
α (°)	85.709(3)	68.166(2)	69.271(2)	71.1684(6)
β (°)	78.946(2)	79.128(2)	76.567(2)	84.4591(5)
γ (°)	69.251(3)	75.546(2)	78.6270(10)	66.4561(6)
<i>V</i> (Å ³)	4435.9(2)	2165.92(10)	8407.9(3)	4260.58(4)
<i>Z</i>	2	1	1	1
Temperature (K)	100(2)	100(2)	100(2)	100(2)
Wavelength (Å)	0.71073	1.54178	0.71073	1.54178
Calculated density (g cm ⁻³)	1.192	1.297	1.180	1.181
Absorption coefficient (mm ⁻¹)	0.281	4.049	0.294	2.303
Transmission factors (min./max.)	0.674 and 1.000	0.711 and 1.000	0.744 and 1.000	0.285 and 1.000
Crystal size (mm ³)	0.14 × 0.07 × 0.01	0.16 × 0.07 × 0.035	0.06 × 0.06 × 0.02	0.18 × 0.08 × 0.035
θ (max) (°)	27.5	68.2	27.5	68.4
Reflections measured	80 640	95 054	110 251	28 571
Unique reflections	19 896	7886	38 753	28 571
<i>R</i> _{int}	0.074	0.0519	0.062	0.057
Reflections with $F^2 > 2\sigma(F^2)$	13 923	7406	24 217	26 256
Number of parameters	975	518	1863	970
<i>R</i> ₁ [$F^2 > 2\sigma(F^2)$]	0.098	0.040	0.088	0.049
<i>wR</i> ₂ (all data)	0.233	0.131	0.256	0.150
GOOF, <i>S</i>	1.127	1.11	1.03	1.04
Largest difference peak and hole (e Å ⁻³)	1.37 and -0.69	1.009 and -0.489	2.04 and -0.87	0.61 and -0.43
τ^c	0.11	0.18	0.12	0.22

Compound	5	6	8-4MeCN ^b
Formula	C ₈₂ H ₉₀ F ₆ N ₂ O ₈ V ₂	C ₈₀ H ₉₀ Cl ₂ N ₂ O ₈ V ₂	C ₉₆ H ₁₀₈ N ₈ O ₈ V ₂
Formula weight	1447.43	1380.31	1711.96
Crystal system	Monoclinic	Monoclinic	Triclinic
Space group	<i>P</i> 2 ₁ / <i>c</i>	<i>P</i> 2 ₁ / <i>n</i>	<i>P</i> $\bar{1}$
Unit cell dimensions			
<i>a</i> (Å)	20.0005(13)	19.7039(9)	12.0966(2)
<i>b</i> (Å)	19.9315(8)	20.0862(7)	12.3373(2)
<i>c</i> (Å)	22.023(2)	20.6921(10)	17.8971(3)
α (°)	90	90	90.8728(8)
β (°)	116.080(10)	113.114(5)	107.9966(7)
γ (°)	90	90	99.2458(8)
<i>V</i> (Å ³)	7885.5(11)	7532.0(6)	2501.28(7)
<i>Z</i>	4	4	1
Temperature (K)	100(2)	100(2)	150(2)
Wavelength (Å)	0.71075	1.54184	0.71073
Calculated density (g cm ⁻³)	1.219	1.217	1.137
Absorption coefficient (mm ⁻¹)	0.305	3.160	0.243
Transmission factors (min./max.)	0.555 and 1.000	0.738 and 1.000	0.974 and 0.990
Crystal size (mm ³)	0.12 × 0.02 × 0.01	0.150 × 0.030 × 0.005	0.11 × 0.06 × 0.04
θ (max) (°)	25.0	66.13	28.3
Reflections measured	86 670	68 213	29 287
Unique reflections	13 936	13 175	12 217
<i>R</i> _{int}	0.1918	0.1107	0.036
Reflections with $F^2 > 2\sigma(F^2)$	6929	5544	8563
Number of parameters	886	791	591
<i>R</i> ₁ [$F^2 > 2\sigma(F^2)$]	0.096	0.085	0.059
<i>wR</i> ₂ (all data)	0.192	0.247	0.185
GOOF, <i>S</i>	1.02	1.02	1.03
Largest difference peak and hole (e Å ⁻³)	1.14 and -0.71	0.420 and -0.378	0.87 and -0.28
τ^c	0.43	0.38	0.28

^a Ref. 24. ^b For 8: data collected on a Bruker APEX 2 CCD diffractometer at Daresbury SRS station 9.8 ($\lambda = 0.6710$ Å). ^c $\tau = (\beta - \alpha)/60$.¹⁴

Conflicts of interest

There are no conflicts to declare.

Acknowledgements

We thank the China Scholarship Council (CSC) for a PhD Scholarship to TX. The EPSRC Mass Spectrometry Service (Swansea, UK) and the EPSRC National X-ray Crystallography Service (Southampton) are thanked for data collection. CR also thanks the EPSRC (grant EP/S025537/1) for financial support and the British Council for funding a workshop in Novosibirsk. We also thank Dr Orlando Santoro for useful discussion. NVS and IES thank the Ministry of Science and Higher Education of Russia (#AAAA-A17-117041710085-9), and Dr. M. A. Matsko for the GPC measurements.

References

- 1 T. Czigány and F. Ronkay, *EXPRESS Polym. Lett.*, 2020, **14**, 510–511.
- 2 For reviews, see (a) O. Dechy-Cabaret, B. Martin-Vaca and D. Bourissou, *Chem. Rev.*, 2004, **104**, 6147–6176; (b) M. Labet and W. Thielemans, *Chem. Soc. Rev.*, 2009, **38**, 3484–3504; (c) C. M. Thomas, *Chem. Soc. Rev.*, 2010, **39**, 165–173; (d) A. Arbaoui and C. Redshaw, *Polym. Chem.*, 2010, **1**, 801–826; (e) Y. Sarazin and J.-F. Carpentier, *Chem. Rev.*, 2015, **115**, 3564–3614 and references therein.
- 3 (a) M. Cozzolino, V. Leo, C. Tedesco, M. Mazzeo and M. Lamberti, *Dalton Trans.*, 2018, **47**, 13229–13238; (b) C. Redshaw, *Catalysts*, 2017, **7**, 165–176; (c) B. Antelmann, M. H. Chisholm, S. S. Iyer, J. C. Huffman, D. Navarro-Llobet, M. Pagel, W. J. Simonsick and W. Zhong, *Macromolecules*, 2001, **34**, 3159–3175; (d) W. Braune and J. Okuda, *Angew. Chem., Int. Ed.*, 2003, **42**, 64–68.
- 4 (a) F. Ge, Y. Dan, Y. Al-Khafaji, T. J. Prior, L. Jiang, M. R. J. Elsegood and C. Redshaw, *RSC Adv.*, 2016, **6**, 4792–4802; (b) C. Redshaw, *Dalton Trans.*, 2016, **45**, 9018–9030; (c) H. Ishikura, R. Neven, T. Lange, A. Galetová, B. Blom and D. Romano, *Inorg. Chim. Acta*, 2021, **515**, 120047.
- 5 (a) Y. Onishi, S. Katao, M. Fujiki and K. Nomura, *Organometallics*, 2008, **27**, 2590–2596; (b) A. Arbaoui, D. Homden, C. Redshaw, J. A. Wright, S. H. Dale and M. R. J. Elsegood, *Dalton Trans.*, 2009, 8911–8922; (c) S. Zhang and K. Nomura, *J. Am. Chem. Soc.*, 2010, **132**, 4960–4965; (d) K. Nomura, A. Igarashi, S. Katao, W. Zhang and W.-H. Sun, *Inorg. Chem.*, 2013, **52**, 2607–2614; (e) X.-Y. Tang, A. Igarashi, W.-H. Sun, A. Inagaki, J. Liu, W. Zhang, Y.-S. Li and K. Nomura, *Organometallics*, 2014, **33**, 1053–1060; (f) N. Diteepeng, X. Tang, X. Hou, Y.-S. Li, K. Phomphrai and K. Nomura, *Dalton Trans.*, 2015, **44**, 12273–12281; (g) K. Nomura, M. Oshima, T. Mitsudome, H. Harakawa, P. Hao, K. Tsutsumi, G. Nagai, T. Ina, H. Takaya, W.-H. Sun and S. Yamazoe, *ACS Omega*, 2017, **2**, 8660–8673; (h) G. Zanchin, L. Vendier, I. Pierro, F. Bertini, G. Ricci, C. Lorber and G. Leone, *Organometallics*, 2018, **37**, 3181–3195; (i) G. Zanchin, F. Bertini, L. Vendier, G. Ricci, C. Lorber and G. Leone, *Polym. Chem.*, 2019, **10**, 6200–6216.
- 6 D. M. Homden and C. Redshaw, *Chem. Rev.*, 2008, **108**, 5086–5130.
- 7 C. Redshaw, M. Walton, K. Michiue, Y. Chao, A. Walton, P. Elo, V. Sumerin, C. Jiang and M. R. J. Elsegood, *Dalton Trans.*, 2015, **44**, 12292–12303.
- 8 C. Redshaw, M. Rowan, L. Warford, D. M. Homden, A. Arbaoui, M. R. J. Elsegood, S. H. Dale, T. Yamato, C. P. Casas, S. Matsui and S. Matsuura, *Chem. – Eur. J.*, 2007, **13**, 1090–1107.
- 9 B. Masci, in *Calixarenes*, ed. M.-Z. Asfari, V. Böhmer, J. Harrowfield, J. Vicens and M. Saadioui, Springer, Netherlands, 2001, ch. 12.
- 10 C. Redshaw, M. Walton, D. S. Lee, C. Jiang, M. R. J. Elsegood and K. Michiue, *Chem. – Eur. J.*, 2015, **21**, 5199–5210.
- 11 See for example, (a) M. A. Woodruff and D. W. Hutmacher, *Prog. Polym. Sci.*, 2010, **35**, 1217–1256; (b) Y. F. Al-Khafaji and F. H. Hussein, in *Green and Sustainable Advanced Materials: Processing and Characterization*, ed. S. Ahmed and C. M. Hussain, Wiley, 2018, ch. 6.
- 12 M. Bochmann, G. Wilkinson, G. B. Young, M. B. Hursthouse and K. M. A. Malik, *J. Chem. Soc., Dalton Trans.*, 1980, 1863–1871.
- 13 D. M. Miller-Shakesby, S. Nigam, D. L. Hughes, E. Lopez-Estelles, M. R. J. Elsegood, C. J. Cawthorne, S. J. Archibald and C. Redshaw, *Dalton Trans.*, 2018, **47**, 8992–8999; W. Clegg, M. R. J. Elsegood, V. C. Gibson and C. Redshaw, *J. Chem. Soc., Dalton Trans.*, 1998, 3037–3039; N. Li, J.-J. Liu, J.-W. Sun, B.-X. Dong, L.-Z. Dong, S.-J. Yao, Z. Xin, S.-L. Li and Y.-Q. Lan, *Green Chem.*, 2020, **22**, 5325–5332; X.-X. Yang, W.-D. Yu, X.-Y. Yi and C. Liu, *Inorg. Chem.*, 2020, **59**, 7512–7519.
- 14 A. W. Addison, T. N. Rao, J. Reedijk, J. van Rijn and G. C. Verschoor, *J. Chem. Soc., Dalton Trans.*, 1984, 1349–1356.
- 15 T. Moriuchi and T. Hirao, *Coord. Chem. Rev.*, 2011, **255**, 2371–2377.
- 16 (a) D. D. Devore, J. D. Lichtenhan, F. Takusagawa and E. A. Maatta, *J. Am. Chem. Soc.*, 1987, **109**, 7408–7416; (b) E. A. Maatta, *Inorg. Chem.*, 1984, **23**, 2560–2561.
- 17 M. Lutz, H. Hagen, A. M. M. Schreurs and G. Van Koten, *Acta Crystallogr., Sect. C: Cryst. Struct. Commun.*, 1999, **55**, 1636–1639.
- 18 (a) P. Slavík and P. Lhoták, *Tetrahedron Lett.*, 2018, **59**, 1757–1759; (b) P. Slavík, H. Dvořáková, M. Krupička and P. Lhoták, *Org. Biomol. Chem.*, 2018, **16**, 838–843.
- 19 See for example, (a) K. Ding, M. O. Miranda, B. Moscato-Goodpaster, N. Ajellal, L. E. Breyfogle, E. D. Hermes, C. P. Schaller, S. E. Roe, C. J. Cramer, M. A. Hillmyer and W. B. Tolman, *Macromolecules*, 2012, **45**, 5387–5396; (b) M. Normand, V. Dorcet, E. Kirillov and J.-F. Carpentier, *Organometallics*, 2013, **32**, 1694–1709; (c) Y. Huang, W. Wang, C.-C. Lin, M. P. Blake, L. Clark, A. D. Schwarz and P. Mountford, *Dalton Trans.*, 2013, **42**, 9313–9324; (d) A. Thevenon, C. Romain, M. S. Bennington, A. J. P. White, H. J. Davidson, S. Brooker and C. K. Williams, *Angew. Chem., Int. Ed.*, 2016, **55**, 8680–8685.



- 20 (a) Q. Hu, S.-Y. Jie, P. Braunstein and B.-G. Lia, *Chin. J. Polym. Sci.*, 2020, **38**, 240–247; (b) M. A. Woodruff and D. W. Hutmacher, *Prog. Polym. Sci.*, 2010, **35**, 1217–1256; (c) T. Wu, Z. Wei, Y. Ren, Y. Yu, X. Leng and Y. Li, *Polym. Degrad. Stab.*, 2018, **155**, 173–182; (d) M. T. Hunley, N. Sari and K. L. Beers, *ACS Macro Lett.*, 2013, **2**, 375–379; (e) Z. Sun, Y. Zhao, O. Santoro, M. R. J. Elsegood, E. V. Bedwell, K. Zahra, A. Walton and C. Redshaw, *Catal. Sci. Technol.*, 2020, **10**, 1619–1639.
- 21 I. E. Soshnikov, N. V. Semikolenova, A. A. Shubin, K. P. Bryliakov, V. A. Zakharov, C. Redshaw and E. P. Talsi, *Organometallics*, 2009, **28**, 6714–6720; I. E. Soshnikov, N. V. Semikolenova, K. P. Bryliakov, A. A. Shubin, V. A. Zakharov, C. Redshaw and E. P. Talsi, *Macromol. Chem. Phys.*, 2009, **210**, 542–548; I. E. Soshnikov, N. V. Semikolenova, K. P. Bryliakov, V. A. Zakharov, C. Redshaw and E. P. Talsi, *J. Mol. Catal. A: Chem.*, 2009, **303**, 23–29.
- 22 (a) B. Masci, *J. Org. Chem.*, 2001, **66**, 1497–1499; (b) B. Dhawan and C. D. Gutsche, *J. Org. Chem.*, 1983, **48**, 1536–1539.
- 23 Despite repeated attempts, the elemental analysis results for this acetonitrile solvate were the closest we could obtain.
- 24 *SAINT and APEX 2 software for CCD diffractometers*, Bruker AXS Inc., Madison, USA, 2006.

